



NOISE-INDUCED INTERMITTENCY IN CELLULAR PATTERN-FORMING SYSTEMS

SCOTT GASNER, PETER BLOMGREN and ANTONIO PALACIOS
*Nonlinear Dynamical Systems Group,
Department of Mathematics and Statistics,
San Diego State University,
San Diego, CA 92182-7720, USA*

Received May 15, 2006; Revised June 19, 2006

We study the effects of thermal noise in a stochastic, Langevin formulation, of a spatio-temporal pattern-forming Partial Differential Equation (PDE) model with circular domain. Modification of a recently developed numerical integration scheme reveals that the pattern-forming model exhibits, in the presence of noise, a greater tendency towards dynamic states and towards intermittent patterns in which ordered states appear randomly, preceded and succeeded by disorganized states. In order to gain additional insight, we focus on a region of parameter space where the patterns of the deterministic system arise from the steady-state interaction of two pairs of modes with wave numbers in a 1:2 ratio. Analysis of the associated stochastic normal form equations allows us to explain the underlying bifurcations of the noise-induced patterns, some of which had only been observed, until now, in laboratory experiments.

Keywords: Spatio-temporal patterns; cellular flames; bifurcation.

1. Introduction

Noise is ubiquitous to the physical world. Historically, it has been considered a nuisance to scientists and engineers who have used considerable effort to suppress it. In more recent years the constructive effects of noise have been examined. In particular, the introduction of noise in a dynamical system can result in organized behavior that does not exist in the absence of noise. An example is stochastic resonance; a phenomenon where an unobservable weak signal can be amplified by noise of the proper intensity to the point where it becomes observable [McNamara *et al.*, 1988]. Another example is the formation of stochastic limit cycles about equilibria of heteroclinic and homoclinic connections. For instance, consider the dynamics of a particle moving along a double-well potential, described by the unforced Duffing oscillator $\ddot{x} = -\dot{x} + x - x^3 + \xi(t)$, where $\xi(t)$ represents a Gaussian white noise function. In the absence of noise, i.e. when $\xi(t) = 0$,

the particle will quickly settle into one of the two equilibrium states represented by the minima of the potential function, see Fig. 1.

In the presence of noise, however, the noise intensity might be too small to change the eigenvalues of a system, but large enough to keep the solution from approaching an equilibrium. Thus the solution will linger around an equilibrium only for finite and random amounts of time, as is now shown in Fig. 2.

In spatially-extended systems, equilibrium points might have a spatial structure, leading to steady-states in the form of ordered patterns. In those systems, stochastic limit cycles can lead to intermittent patterns in which one or more ordered patterns appear randomly as the system dynamics approaches a neighborhood of an equilibrium state. In this work, we consider stochastic limit cycles but with particular interest on pattern-forming systems that can exhibit cellular structures.

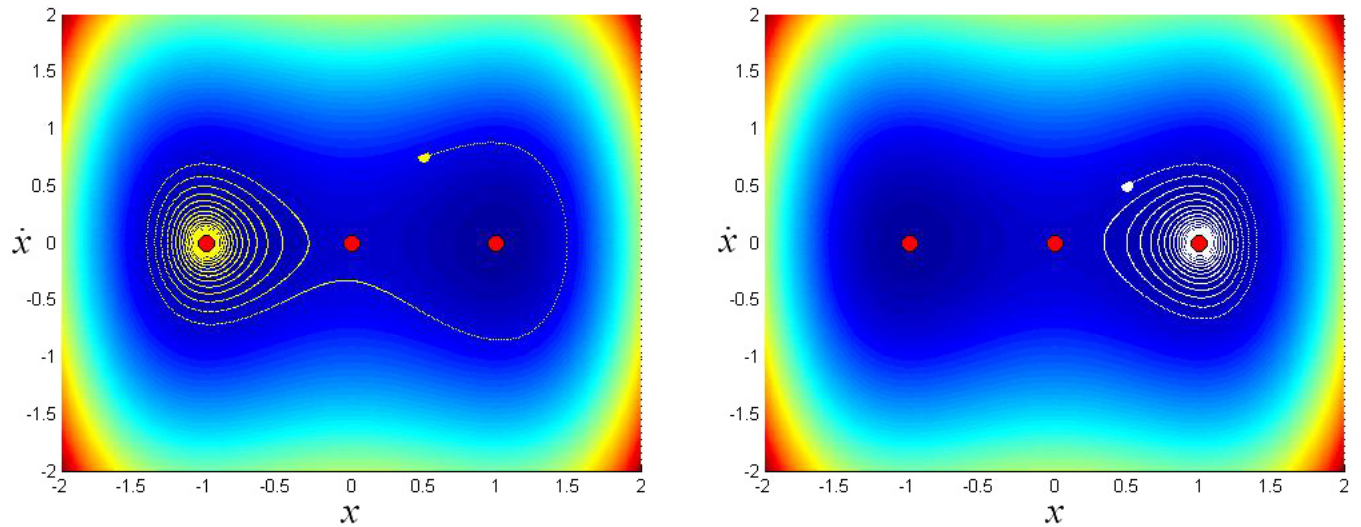


Fig. 1. Motion of a particle on a double-well potential function. In the absence of noise, the system dynamics quickly settles into an equilibrium point. Which equilibrium point is selected, (left) or (right), depends on the initial conditions.

Such patterns are common features of many non-linear phenomena. In material science, they appear in mud cracking patterns, in ceramics and minerals [Aboav, 1970], in polycrystalline metals, in soap suds, and in magnetic bubbles [Glazier *et al.*, 1992]. They are also found in honey combs [Kepler, 1966; Dormer, 1980], in flame fronts [Gorman *et al.*, 1994], and in vibrated granular systems [Tsimring, 1997]. Understanding the mechanisms that govern the spatial and temporal evolution of cellular patterns, and their response to noise, is important because such

knowledge can lead, for instance, to novel designs and developments of new materials.

2. Modeling

To investigate the effects of noise on cellular patterns, we consider in this work a stochastic (Langevin) version of a generic example of a cellular-pattern-forming dynamical system, known as the Kuramoto–Sivashinsky (KS) equation

$$\frac{\partial u}{\partial t} = \eta_1 u - (1 + \nabla^2)^2 u - \eta_2 (\nabla u)^2 - \eta_3 u^3 + \xi(\mathbf{x}, t), \quad (1)$$

where $u = u(\mathbf{x}, t)$ represents the perturbation of a planar front (which is normally assumed to be a flame front) in the direction of propagation, η_1 measures the strength of the perturbation force, η_2 is a parameter associated with growth in the direction normal to the domain (burner) of the front, $\eta_3 u^3$ is a term that is added [Chate *et al.*, 1993] to help stabilize the numerical integration, and $\xi(\mathbf{x}, t)$ represents Gaussian white noise, which models thermal fluctuations, dimensionless in space and time. We assume $\xi(\mathbf{x}, t)$ to be distributed with zero mean $\langle \xi(\mathbf{x}, t) \rangle = 0$, and to be uncorrelated over space and time, i.e. $\langle \xi(\mathbf{x}, t) \xi(\mathbf{x}', t') \rangle = 2D \delta(\mathbf{x} - \mathbf{x}') \delta(t - t')$, where D is a measure of the intensity of the noise, $\langle \cdot \rangle$ represents the time-average over a range of observations.

The Kuramoto–Sivashinsky equation describes the perturbations of a uniform wave front by thermo-diffusive instabilities. It has been studied in different contexts by Cross and Hohenberg

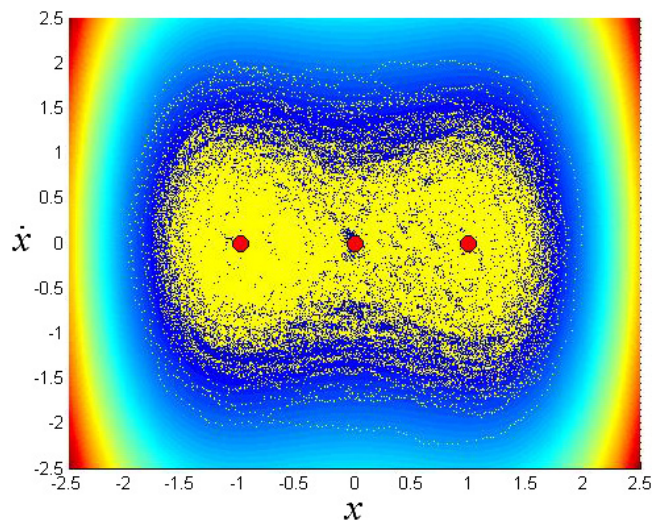


Fig. 2. Motion of a particle on a double-well potential function subject to noise. The system dynamics now lingers intermittently between the two equilibrium states of the deterministic system, independently of initial conditions.

[Cross *et al.*, 1993], Armbruster, Guckenheimer and Holmes [Armbruster *et al.*, 1988], and by Hyman and Nicolaenko [Hyman *et al.*, 1986]. In the context of combustion of premixed gases, in particular, thermo-diffusive instability is caused by the interaction of diffusion and conduction of a gas flame [Palacios *et al.*, 1997]. These studies show that, overall, thermo-diffusive instabilities can lead to complex stationary and dynamic cellular patterns, which emerge from the geometry of the domain through the universal properties of symmetry-breaking bifurcations. Another example of a pattern-forming system relevant to this work is that of Faraday waves [Faraday, 1831]. In that system, cellular patterns similar to those of combustion flames can be created on the free surface of a fluid layer that is periodically vibrated if the amplitude of the driving force is large enough to overcome the dissipative effect of fluid viscosity.

2.1. Numerical stochastic method

The first numerical scheme for integrating the KS model equation (1), without noise, and over a two-dimensional circular domain, was completed by Zhang *et al.* [1999] through the use of Distributed Approximating Functionals (DAFs). The DAF approach allowed circumvention of certain coordinate singularities that had previously made the integration of the KS model sensitive to the accuracy of the spatial derivatives. Shortly after the scheme was completed, several stationary cellular patterns with multiple rings and a few dynamic states such as single rings of rotating cells were observed but only for brief periods of time. The resulting scheme was based on a local linearization of the nonlinear terms in the KS equation and was unstable for long-term simulations. In recent work, we developed a Crank–Nicolson based integration scheme that solves the numerical instability problem [Blomgren *et al.*, 2005a]. The improved scheme has helped us numerically simulate [Blomgren *et al.*, 2005b], for long periods of time, a wide variety of stationary and dynamic cellular patterns, many of which had only been previously observed in laboratory experiments [Gorman *et al.*, 1994]. In the present paper we build on our previous numerical scheme [Blomgren *et al.*, 2005a] in order to develop a new method to integrate the stochastic version of the KS model (1). Next we summarize the essentials and describe the modifications introduced for this paper. The scheme employs

distributed approximating functionals for calculating the derivatives with respect to space [Zhang *et al.*, 1999]. The scheme is second order in time, based on the Crank–Nicolson scheme [Crank *et al.*, 1947], and is linearly unconditionally A-stable. In order to numerically resolve the nonlinearity, the scheme employs a Newton iteration in each time-step, in which the resulting sequence of linear systems are solved using the preconditioned Bi-CGSTAB method [Vorst, 1992]. The preconditioner is chosen to be the unchanging linear part of the discretized operator.

Let $\mathbf{x} = (r, \phi)$ represent the polar coordinates of the circular domain, see Fig. 3, and let $F(\mathbf{x}, t, u(\mathbf{x}, t), \xi(\mathbf{x}, t))$ represent the right-hand side of (1), so that $u_t(\mathbf{x}, t) = F(\mathbf{x}, t, u(\mathbf{x}, t), \xi(\mathbf{x}, t))$.

Furthermore, for this discussion, we decompose the right-hand side, $F(\mathbf{x}, t, u(\mathbf{x}, t), \xi(\mathbf{x}, t))$ into deterministic and stochastic parts, e.g.

$$F(\mathbf{x}, t, u(\mathbf{x}, t), \xi(\mathbf{x}, t)) = F_{\text{det}}(\mathbf{x}, t, u(\mathbf{x}, t)) + F_{\text{sto}}(\mathbf{x}, t, \xi(\mathbf{x}, t)) \quad (2)$$

where, $F_{\text{sto}}(\mathbf{x}, t, \xi(\mathbf{x}, t)) = \xi(\mathbf{x}, t)$. Since the stochastic term is uncorrelated (white) in time, and independent of $u(\mathbf{x}, t)$, we can evaluate the term in the center of the time-step, i.e. at time $t + (h/2)$, thus solving (2) using the Crank–Nicolson

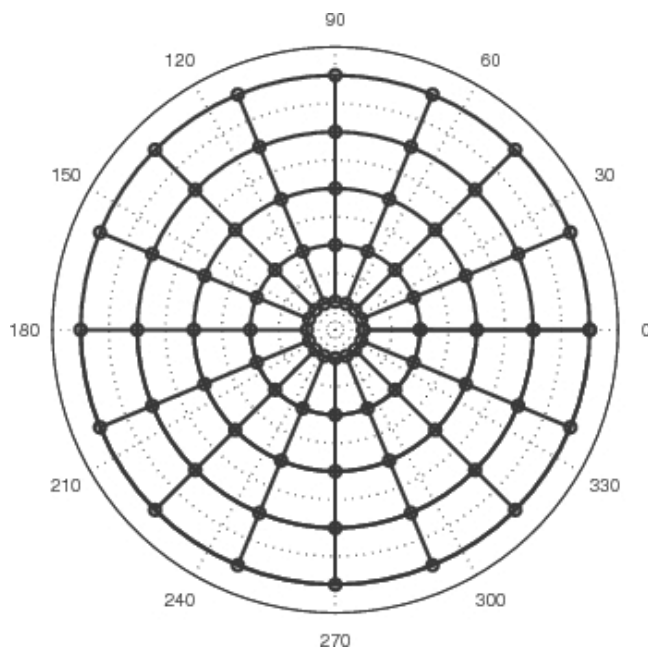


Fig. 3. The polar grid. Notice that the innermost points are located at a radius $r = dr/2$; hence there is no computational point at the center of the grid. The radial spacing is dr . In our computations we use 32 radial points and 64 azimuthal points, i.e. $dr = R/32.5$ and $d\phi = 2\pi/64$.

scheme [Crank *et al.*, 1947] we get an equation for the unknown $u(\mathbf{x}, t + h)$

$$\begin{aligned} & \frac{u(\mathbf{x}, t + h) - u(\mathbf{x}, t)}{h} \\ &= \frac{F_{\text{det}}(\mathbf{x}, t, u(\mathbf{x}, t))}{2} + \frac{F_{\text{det}}(\mathbf{x}, t + h, u(\mathbf{x}, t + h))}{2} \\ & \quad + F_{\text{sto}}\left(\mathbf{x}, \frac{t+h}{2}, \xi\left(\mathbf{x}, \frac{t+h}{2}\right)\right). \end{aligned} \quad (3)$$

Equation (3) leads to a nonlinear system of equations of the form $G(u(\mathbf{x}, t + h)) = 0$, which we solve for $u(\mathbf{x}, t + h)$ using Newton’s method as follows

$$\begin{aligned} \mathbf{u}^{n+1}(\mathbf{x}, t + h) &= \mathbf{u}^n(\mathbf{x}, t + h) - [\delta\mathbf{G}(\mathbf{u}^n(\mathbf{x}, t + h))]^{-1} \\ & \quad \cdot \mathbf{G}(\mathbf{u}^n(\mathbf{x}, t + h)), \\ \mathbf{u}^0(\mathbf{x}, t + h) &= \mathbf{u}(\mathbf{x}, t) \end{aligned}$$

Here $\delta\mathbf{G} = \nabla_u \mathbf{G}(\mathbf{u}^n(\mathbf{x}, t + h))$ is the Jacobian. Since $F_{\text{sto}}(\mathbf{x}, t + h/2, \xi(\mathbf{x}, t + h/2))$ does not depend on $u(\mathbf{x}, t + h)$, it only affects the linear system as a constant addition to $G(u(\mathbf{x}, t + h))$, with no contribution to the Jacobian. In each step of the Newton-iteration we solve the linear system

$$[\delta\mathbf{G}(\mathbf{u}^n(\mathbf{x}, t + h))]\delta\mathbf{u} = \mathbf{G}(\mathbf{u}^n(\mathbf{x}, t + h)). \quad (4)$$

In our simulations, the grid is subdivided into $N_r = 32$ radial points, and $N_\phi = 64$ azimuthal points, leading to a nearly dense 2048×2048 systems. We solve these systems using the preconditioned biconjugate gradient stabilized method (Bi-CGSTAB) [Barret *et al.*, 1994].

2.2. Simulations

Computer simulations indicate a greater tendency towards stationary states (as opposed to dynamic states) in noise-free simulations of the KS model (1). Stationary states are patterns with petal-like cellular structures and well-defined spatial symmetries. Figure 4 illustrates a few examples. Dynamic states are patterns in which the cells move, either individually or in ring configurations.

As the radius of the circular domain increases, the typical ordered state that appears changes from a single ring of cells to concentric rings of cells. Occasionally, dynamic states are also observed in the transition from one stationary pattern to another. In previous work [Palacios *et al.*, 1997], we studied the selection mechanism behind this transition; in particular, we explained why cellular patterns consist of rings of cells and also determined the mechanisms that lead to some dynamic states. More specifically, we found that uniformly rotating and modulated rotating single-ring states with k cells were typically generated by the interaction of two steady-state modes with Fourier wave numbers in a $k:2k$ ratio. We now focus our attention around a 1:2 mode interaction, though the analysis still captures many essential features of the effects of noise on larger patterns. The diagram in Fig. 5 depicts the transition that results from such mode interaction. Without noise, i.e. noise amplitude $D = 0$, a one-cell rotating state (1R) appears in the transition from a one-cell stationary state to a two-cell stationary state, just as predicted by the corresponding 1:2 mode interaction.

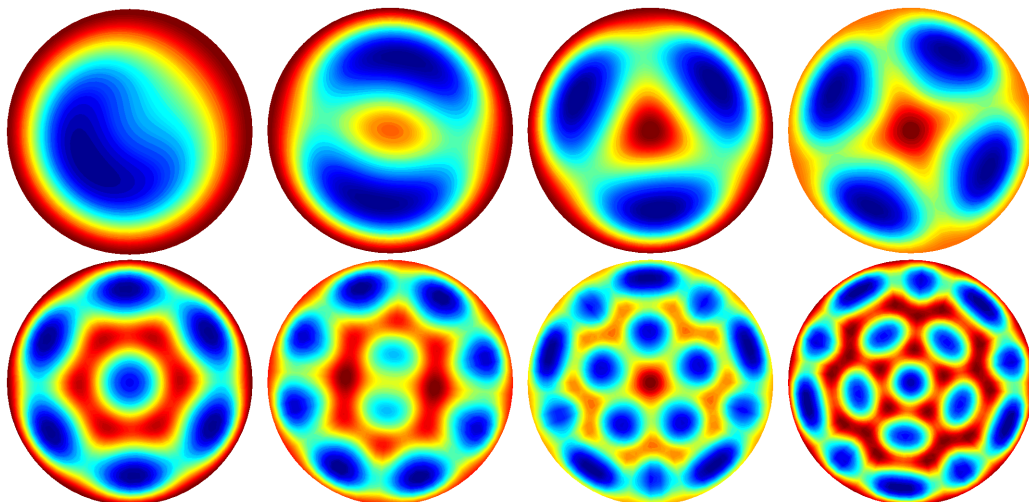


Fig. 4. Representative examples of stationary states found in numerical simulations of the KS model (1), with $\xi(\mathbf{x}, t) = 0$, i.e. without noise.

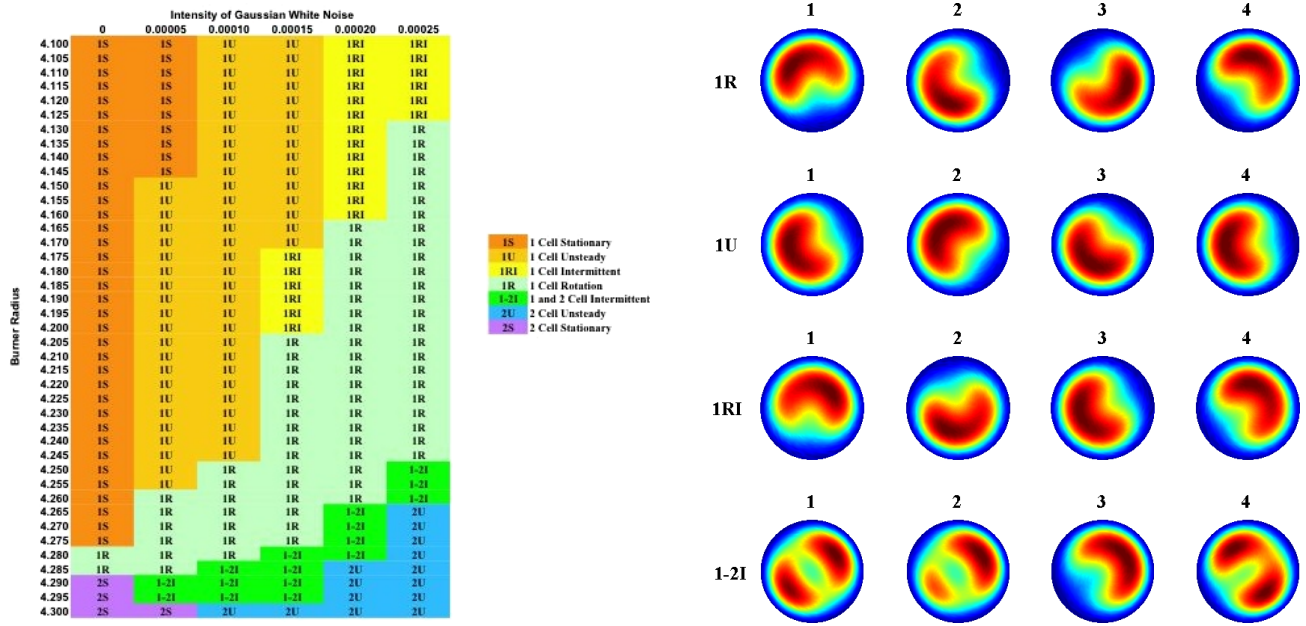


Fig. 5. Generic behavior of the KS model for various parameter values of radius and noise intensity. Notation: 1 = single cell, 2 = 2 cell. S = Stationary, U = Unsteady, I = Intermittent State, R = Rotation. Noise intensity, $D = \sigma^2/2$, is in the range $[0.00, 2.5E-04]$. This range represents low noise levels, relative to the dynamic range of u , which in the Kuramoto-Sivashinsky equation is of order 10. As the noise intensity increases, the radius-parameter range of complex dynamic patterns is extended; when the intensity reaches $D = 1.25 \times 10^{-3}$ no static patterns are observed. For each of these simulations $\eta_1 = 0.32$, $\eta_2 = 1.0$, $\eta_2 = 0.017$, $4.1 \leq \text{radius} \leq 4.35$, and $D \leq 0.5$.

As the noise intensity increases, the domain of existence of the 1R-state increases and additional patterns emerge, see Fig. 5. For very weak noise, an unsteady dynamic pattern (1U) appears between the 1S and 1R states. The 1U pattern does not sustain rotations; instead, the pattern rocks back and forth. With increased noise intensity, a one-cell rotating pattern (1RI), which intermittently changes its direction of rotation, is observed between the 1U and 1R patterns. Near the bifurcation point, where the 1RI state forms, there are two bistable branches of rotating states created by symmetry, one branch for each direction of rotation. Which branch is observed depends mainly on initial conditions. Noise appears to act as a switch, inducing recurrent transitions between these two branches. Between the 1R and 2S (or, for higher noise intensities, 2U) patterns, an intermittent 1-2 cell pattern forms. This dynamic pattern is very peculiar: one of the two cells in the 2S state is extinguished; the remaining one-cell state is short-lived, the pattern immediately splits into a new 2S-state, the orientation of which is roughly a quarter-rotation of the previous 2S-state. Each appearance of the 2S state lasts an irregular amount of time, ranging from a few to several hundreds of frames. This is qualitative evidence of a heteroclinic

connection where the stable (unstable) manifold of a two-cell equilibrium is also the unstable (stable) manifold of another two-cell equilibrium. Until now, this pattern had only been observed in laboratory experiments [Gorman *et al.*, 1994; Stone *et al.*, 1996] but not in computer models. Finally, a 2-cell analogue (2U) of the 1U pattern forms between the 1-2I and 2S patterns.

3. Analysis

3.1. Mode decomposition

In order to explain, quantitatively, the origin and formation mechanisms of the noise-induced intermittent pattern shown in Fig. 5, we perform next a Proper Orthogonal Decomposition [Karhunen, 1946; Loève, 1955; Lumley, 1967; Palacios *et al.*, 1998; Sirovich, 1987a, 1987b, 1987c] analysis of an ensemble, made up of about 4000 computer-simulated spatio-temporal data points (frames), for each individual case. To ensure that the POD steady-state modes contain the correct symmetry properties, we have taken special care of including the average over the symmetry group, $O(2)$, of the experiment, in the ensemble average. In all four cases, the POD analysis reveals that two pairs

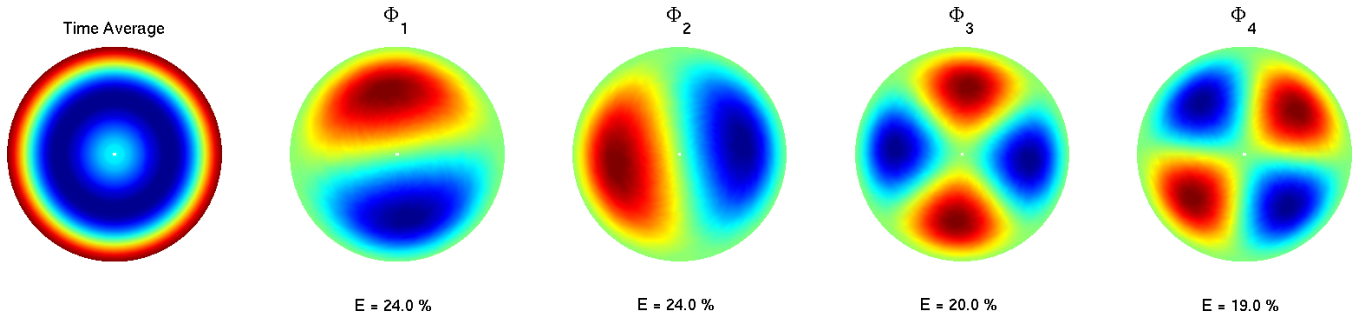


Fig. 6. A proper orthogonal decomposition analysis reveals that all four patterns of Fig. 5 are created from the mutual interaction of two pairs of spatial modes whose wave numbers are in a 1:2 ratio. These modes were obtained using computer-simulated ensembles of 4000 data set points of each individual pattern.

of modes with wave numbers in a 1:2 ratio capture most of the dynamics, see Fig. 6.

The time-average (considered mode Φ_0) is shown first followed by four POD modes, Φ_1 – Φ_4 , with the highest percentage of energy (see Appendix for an exact definition). The actual amount of energy in each mode is indicated below each mode. Each mode shows some amount of symmetry. The symmetry of the time-average, in particular, reflects the $\mathbf{O}(2)$ -symmetry of the burner, even though none of the instantaneous snapshots has this symmetry. This feature is studied in more detail in [Dellnitz *et al.*, 1994]. Φ_1 and Φ_2 show D_1 -symmetry, meaning that one complete revolution leaves them unchanged, while Φ_3 and Φ_4 show D_2 -symmetry, i.e. the patterns are restored after half a revolution. Observe also that the energy is equally distributed among these two pairs of modes, which together capture almost 90% of the original behavior. It follows that intermittent behavior in all three cases is created from the mutual interaction of two invariant eigenspaces, $V_1 = \text{span}\{\Phi_1, \Phi_2\}$ and $V_2 = \text{span}\{\Phi_3, \Phi_4\}$, whose dihedral symmetries are in a 1 : 2 ratio, just as expected from direct inspection of the transition diagram of Fig. 5. We postpone further discussion of the 1RI and 1U patterns until later when we compare results of the POD decomposition with solutions of the associated amplitude equations.

Next we examine results of the POD decomposition of the 1-2I intermittent state. Figure 7 shows the time-dependent coefficients associated with each individual POD mode. To help visualize the actual transitions, we have added two markers, a green circle and a red circle. The time between the green (red) circle and the red (green) define the beginning and end of a 2-cell (1-cell) pattern, respectively. Observe that when the oscillations in

$a_1(t)$ and $a_2(t)$ have large amplitudes relative to those of a_3 and a_4 , the 1-cell pattern shows up. The opposite relation, small amplitude in a_1, a_2 and large amplitude in a_3, a_4 , leads to the appearance of the 2-cell pattern.

The heteroclinic saddle-node connections that underlie the transitions between the 1-cell pattern and the 2-cell state, can be observed better in the phase-space portrait of Fig. 8. Black arrows indicate the approximate direction of the flow around the two saddle-nodes that are associated with a 2-cell state, while there are four saddle-nodes that correspond to the 1-cell state. This difference deserves an explanation. Once a 2-cell state appears in the simulations, there is only one distinct orthogonal position in which the same pattern can reappear. On the other hand, a 1-cell state has four orthogonally distinct positions where it can reappear. These geometric facts determine the structure of the phase portrait of Fig. 8.

3.2. Amplitude equations

As was mentioned before, all three intermittent patterns, 1RI, 1U, and 1-2I, emerge from the mutual interaction of two pairs of spatial modes, $\{\Phi_1, \Phi_2\}$ – $\{\Phi_3, \Phi_4\}$, with wave numbers in a 1:2 ratio, while the time evolution of each individual pattern is determined by the amplitude coefficients $a_1(t)$ – $a_4(t)$ that are associated with the spatial modes Φ_1 – Φ_4 , respectively. The amplitude equations that govern the evolution of the time-dependent coefficients are derived from the 1-to-2 Fourier-mode interaction in a system with $\mathbf{O}(2)$ -symmetry, i.e. the symmetry group of rotations and reflections of the circular domain. The deterministic version of these amplitude equations in Birkhoff Normal Form has been thoroughly studied by Armbruster *et al.* [1988]. The

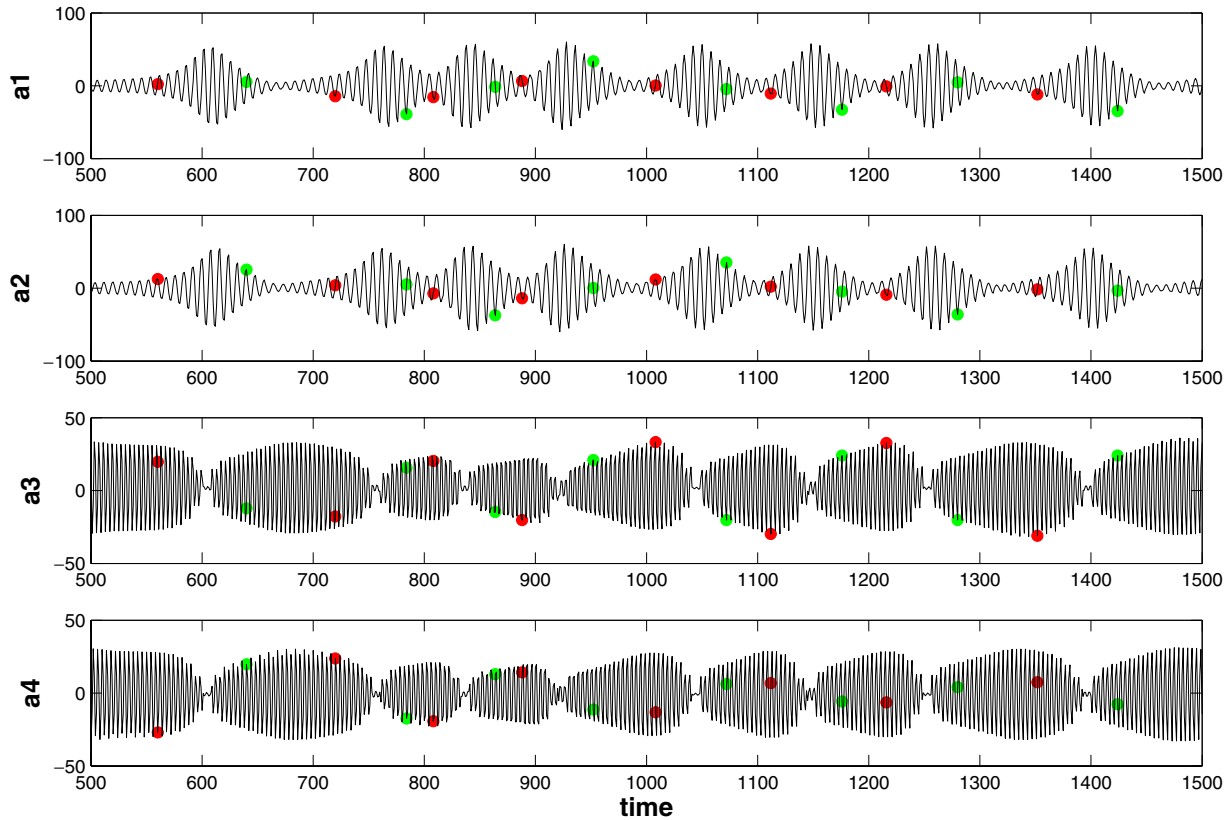


Fig. 7. Amplitude coefficients associated with the POD modes of the intermittent state 1-2I of Fig. 5. Horizontal axis denotes time. Markers indicate beginning (green) and end (red) of a 2-cell pattern.

Langevin version below

$$\begin{aligned} \dot{z}_1 &= \bar{z}_1 z_2 + z_1(\mu_1 + e_{11}|z_1|^2 + e_{12}|z_2|^2) + \varepsilon\eta_1(t) \\ \dot{z}_2 &= \pm z_1^2 + z_2(\mu_2 + e_{21}|z_1|^2 + e_{22}|z_2|^2) + \varepsilon\eta_2(t), \end{aligned} \tag{5}$$

where $\eta_1(t)$ and $\eta_2(t)$ are Gaussian white noise functions, uncorrelated with zero mean and with amplitude ε , has also been considered by Stone and Holmes [1991] in a study of the effects of noise on heteroclinic cycles. We will draw on their work when we study the 1-2I intermittent pattern; but we will also extend the analysis to other regions of parameter space in order to explain the evolution of the 1RI and 1U intermittent patterns. We start with the 1R pattern. According to the transition diagram of Fig. 5, and to the POD relative phase-angles plots of Fig. 10, it is reasonable to associate the temporal evolution of the 1R pattern with that of a traveling wave of the deterministic normal forms, i.e. $\eta_1 = 0$ and $\eta_2 = 0$ in (5). We claim that the 1RI pattern arises from noise perturbations of a traveling wave solution of the normal forms. We prove this claim next. For convenience, we let $z_j = re^{\theta_j i}$ and $\phi = 2\theta_1 - \theta_2$, so that we can rewrite (5) in polar

coordinates

$$\begin{aligned} \dot{r}_1 &= r_1 r_2 \cos \phi + r_1(\mu_2 + e_{11}r_1^2 + e_{12}r_2^2) + \varepsilon\eta_1(t) \\ \dot{r}_2 &= \pm r_1^2 \cos \phi + r_2(\mu_4 + e_{21}r_1^2 + e_{22}r_2^2) + \varepsilon\eta_2(t) \\ \dot{\phi} &= -\left(2r_2 \pm \frac{r_1^2}{r_2}\right) \sin \phi. \end{aligned} \tag{6}$$

Observe that the noise functions η_1 and η_2 do not appear, explicitly, in the last equation in (6), which governs the evolution of the phase-difference variable. We will show that noise can, however, change the evolution of the phase difference through the radial components r_1 and r_2 . Consider the noise-free system: $\eta_1 = 0$ and $\eta_2 = 0$. Traveling Waves (TW) are equilibria of (5) in which the phase difference remains constant, though $\phi_2 \neq 0, \pi$. In physical space, TWs correspond to uniformly rotating patterns produced by evolution equations; e.g. the 1R pattern that appears in simulations of the Kuramoto-Sivashinsky model (1). Following Armbruster *et al.*, traveling waves (of the deterministic system) are created via a pitchfork bifurcation from the π -mixed mode solution ($r_1 \neq 0, r_2 \neq 0, \phi = \pi$) when $2r_4 \pm r_2^2/r_4 = 0$, and $\phi_2 = \pi$, so that they

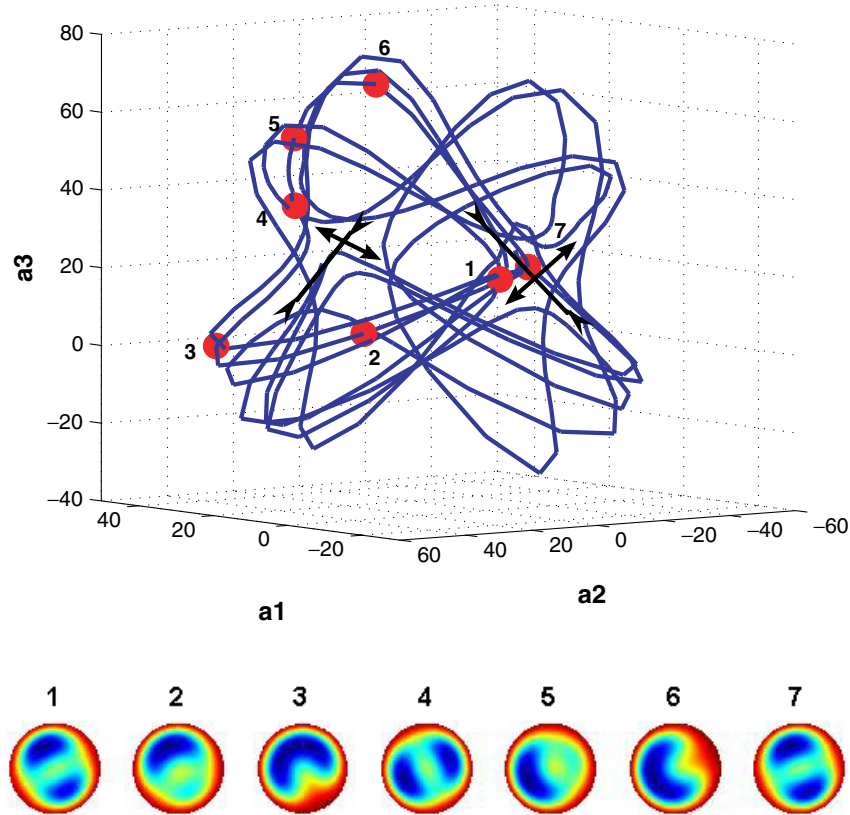


Fig. 8. Phase-space portrait from time-dependent POD coefficients for an intermittent state 1-2I clearly capture saddle-node connections between the stable and unstable manifolds associated with each individual ordered pattern, one with 1-cell and one with 2-cell.

only exist in the “-” case or when $r_1^2 = 2r_2^2$. Letting $e = 4e_{11} + 2e_{12} + 2e_{21} + e_{22}$, it can be shown that TW solutions of (5), without noise, exist and are stable for

$$\begin{aligned}
 & -2\mu_1 - e\mu_1^2 + O(\mu_1^3) < \mu_2 \\
 & < \mu_1 \left(1 + \frac{9(e_{22} - e_{12})}{e - 3(e_{22} - e_{12})} \right) + O(\mu_1^2). \quad (7)
 \end{aligned}$$

Consider now the noisy system. Direct calculations of the equilibria of (6) lead to

$$\lambda r_2 + e r_2^3 + \sigma \eta_3(t) = 0, \quad (8)$$

where $\lambda = 2\mu_1 + \mu_2$ and η_3 is also a Gaussian white noise function, uncorrelated with zero mean, but with amplitude $\sigma = \sqrt{3}\varepsilon$. When $\sigma = 0$, Eq. (8) reduces to the normal form equation for the pitchfork bifurcation that underlie the birth of the TWs of the deterministic system. A more critical observation is the fact that *additive white noise does not modify qualitatively the solution set of a codimension-one, perfect, pitchfork bifurcation* [Juel et al., 1997]. It follows that TW solutions, and their stability properties, of the noisy system (5) necessarily coincide with those of the deterministic,

$\sigma = 0$, system; and Eq. (7) is still valid for the noisy system. But if the 1RI pattern is indeed a noise-perturbed TW, then we seem to have an apparent contradiction: how can noise change the direction of rotation of the 1RI state if noise cannot modify the qualitative properties of the pitchfork bifurcations that lead to traveling waves? To clarify this subtle issue, we need to take into account that equilibria of (6) are now described by a probability density function $p(r_i, t)$. In the case of the pitchfork bifurcation (8), $p(r_2, t)$ is governed by the following Fokker-Planck equation

$$\partial_t p(r_2, t) = -\partial_r (\lambda r_2 + e r_2^3) p(r_2, t) + \frac{\sigma^2}{2} \partial_{rr} p(r_2, t). \quad (9)$$

Traveling waves solutions are described by stationary solutions of (9), which, in turn, yields the stationary probability density function

$$p_s(r_2) = N \exp \left[\left(\frac{2}{\sigma^2} \right) \left(\lambda \frac{r_2^2}{2} + e \frac{r_2^4}{4} \right) \right]. \quad (10)$$

Computer simulations, see Fig. 9, show that this function changes from single to double peaked

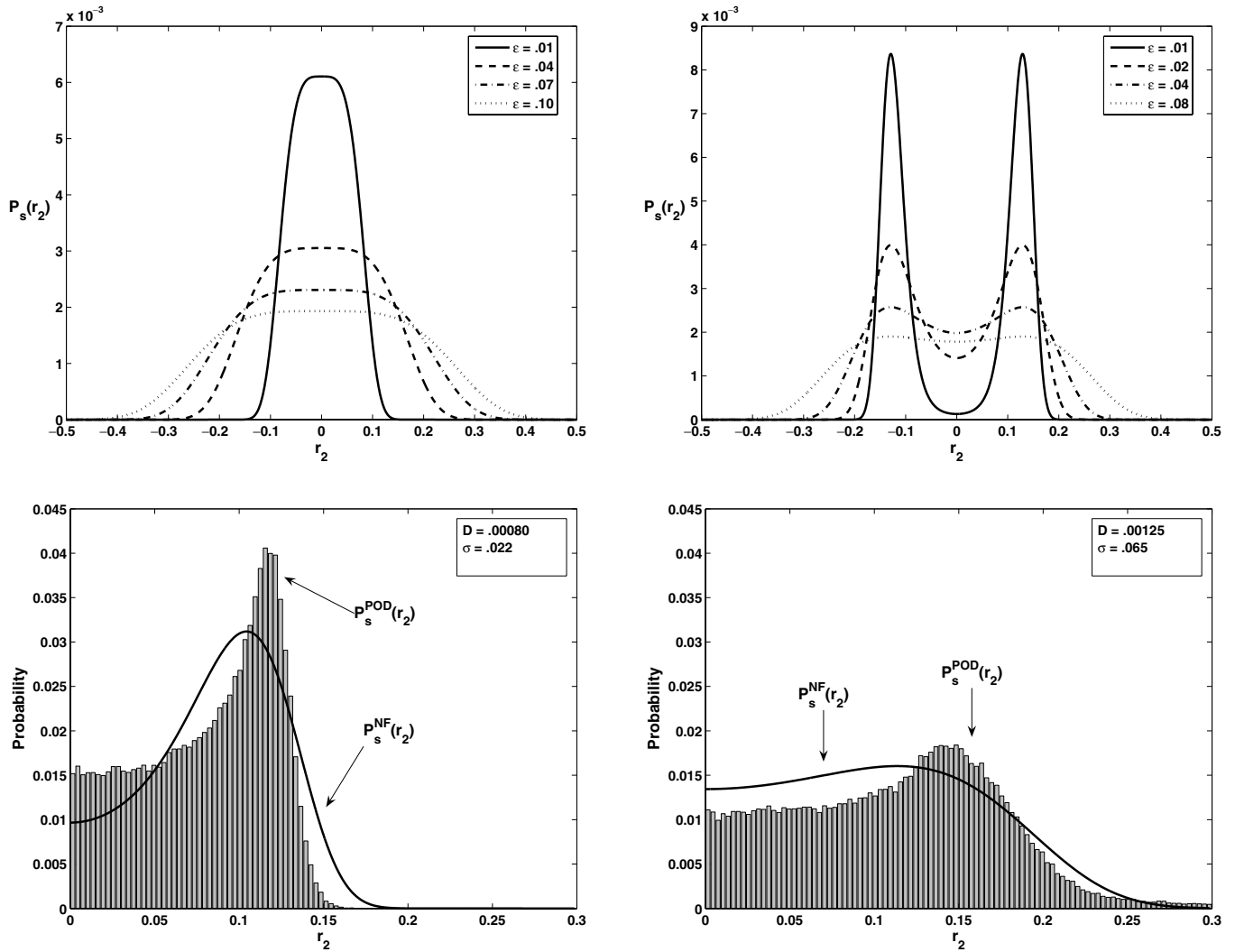


Fig. 9. Stationary probability density of the radial component of the pitchfork bifurcation that leads to TW solutions.

as λ increases across zero. In both cases, $\lambda < 0$ and $\lambda > 0$, the location of the peaks always coincide with the steady states of the deterministic system. As predicted by theory, noise does not modify the qualitative characteristics of the underlying pitchfork bifurcation. However, noise can change the probability distribution around the steady-state $r_2 = 0$. Assuming $\lambda > 0$, we notice that as noise intensity increases from zero, the proportion of time spent by a typical solution of (6) around $r_2 = 0$ increases continuously until it reaches a maximum, at which time the phase-difference angle is no longer at an equilibrium, thus triggering a transition that changes the sign of the phase-difference angle, and ultimately, the direction of rotation of the wave. This cycle of events repeats itself at random time-intervals as the system dynamics in r_2 change back and forth between zero and the values

of the deterministic system. As for the 1U pattern, since standing waves lie on the invariant subspace $\phi = 0$, or $\phi = \pi$, noise perturbations of the radial components r_1 and r_2 cannot destroy the invariance of the subspaces because they do not enter, explicitly, into the dynamics of the phase angle. Consequently, the only possible effect of noise variations in r_1 and r_2 is to create small oscillations in the phase-angle variable ϕ , thus rocking the wave back and forth.

To further verify the validity of our previous assertions, we compare in Fig. 10 the relative phase-angle obtained from the amplitude coefficients associated with each pair of POD modes (see Appendix for an exact definition) with those from the normal form equations. The linear variation of the phase angles of the 1R pattern indicate that this pattern rotates uniformly, in which a negative slope is also

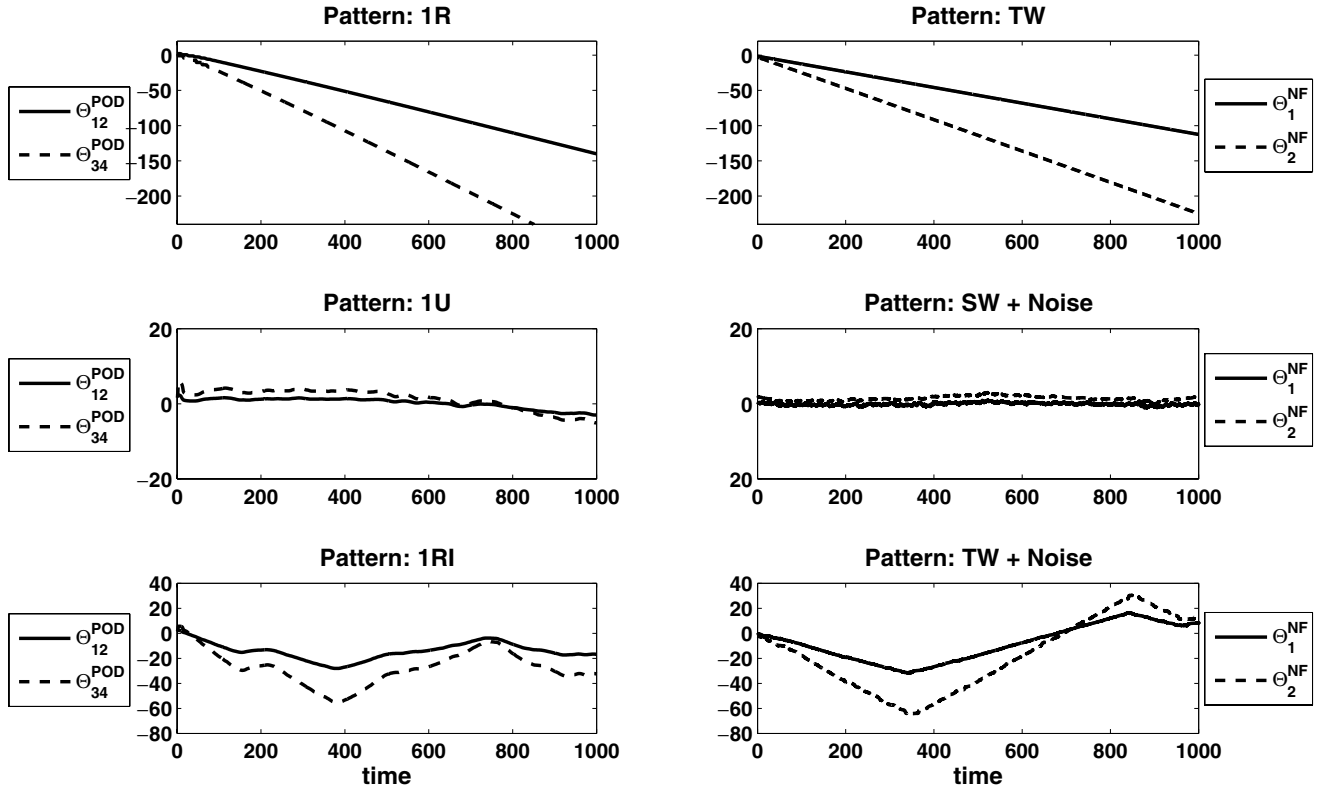


Fig. 10. Comparison of relative phase-angles for the patterns: 1R, 1U and 1RI, obtained from the POD analysis (left) and from the normal form equations (right).

indicative of counter-clockwise rotations. In the 1U state, the phase angles only jiggle back and forth since the pattern does not make any revolutions. In the 1RI pattern, however, the phase angles vary enough to induce rotations but the variations are accompanied with random changes in the direction of rotation.

We now turn our attention to the 1-2I pattern, which brings us back to the work of Stone and Holmes [1991]. Among their findings, most relevant to the analysis of the 1RI pattern, is the realization that certain intermittent states can be described as noise-induced “stochastic limit cycles” that are created from the perturbation of heteroclinic orbits connecting saddle-node equilibria of the deterministic ($\varepsilon = 0$) normal forms. Furthermore, the passage time of a typical orbit lingering near one of these equilibrium points obeys the following probability distribution function

$$P(t) = \frac{2\lambda\Delta(t)e^{-\Delta^2(t)}}{\sqrt{\pi}(1 - e^{-2\lambda t})}, \tag{11}$$

where $\Delta(t) = \delta[(\varepsilon^2/\lambda)(e^{2\lambda t} - 1)]^{-1/2}$, λ is the largest unstable eigenvalue of the equilibrium points, ε is the noise amplitude seen in (5), and δ is the size

of a neighborhood around the equilibrium points. In Fig. 11 we calculate the passage times (vertical bars) using numerical simulations of the 1-2I pattern. The equilibrium points correspond to the

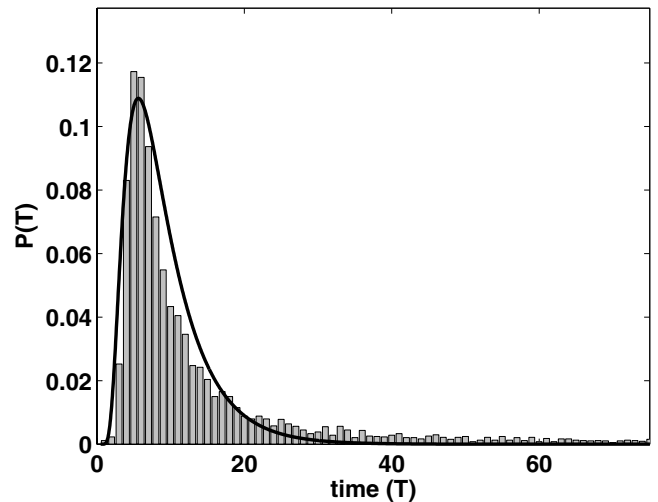


Fig. 11. Passage times calculated (vertical bars) from numerical simulations of the 1-2I intermittent pattern and, (bold curve) by fitting the probability distribution function of Eq. (11) with parameters: $\lambda = 0.28$, $\varepsilon = 0.030$, and $\delta = 0.20$.

two different orientations of the two-cell states that appear intermittently. The bold curve is a fitting of the probability distribution function $P(t)$ given by Eq. (11).

Figure 12 depicts the phase-space projection of a typical trajectory of (5) onto the first two components of z_1 and the x -component of z_2 , which are the analogous of the POD amplitude coefficients a_1 , a_2 and a_3 , respectively. The reconstructed pattern, calculated through the following equation,

$$U_{\text{rec}}(\mathbf{x}, t_i) = \sum_{k=1}^4 z_k(t_i) \Phi_k(\mathbf{x}), \quad i = 1, \dots, M,$$

where M is the size of the ensemble, 4000 frames in this case, is also shown immediately below the phase-space projection. The resemblance of the phase space with the POD phase-space projection of

Fig. 8 is clear. More importantly, the reconstructed intermittent state is qualitatively similar, up to a rotation, to the PDE simulations. The cell rotates uniformly and, intermittently changes direction of rotation. In summary, numerical calculations, the curve fitting of $P(t)$, and the phase-space reconstruction of Fig. 12, are strong evidence that the 1-2I intermittent state is indeed a stochastic limit cycle created from the perturbation of a heteroclinic connection. Such connections would be unobservable under noise-free conditions.

As a final remark, we wish to emphasize that more complex intermittent transitions are also found in simulations of the KS model (1). For instance, Fig. 13 shows noise-induced intermittent behavior in a two-ring configuration, which are found in computer simulations of the Kuramoto–Sivashinsky model (1) in the parameter region

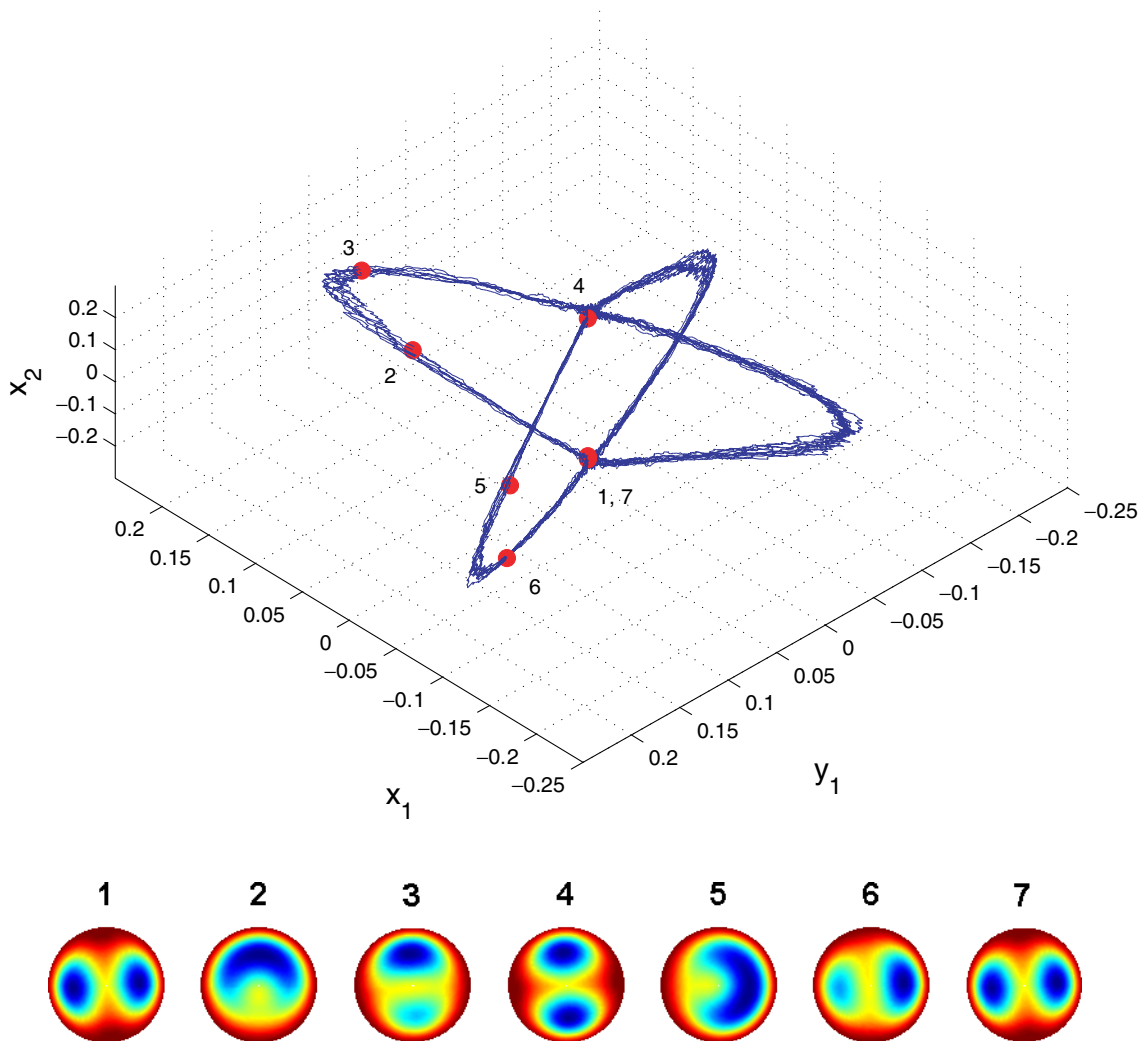


Fig. 12. Phase-space portrait from normal form equations.

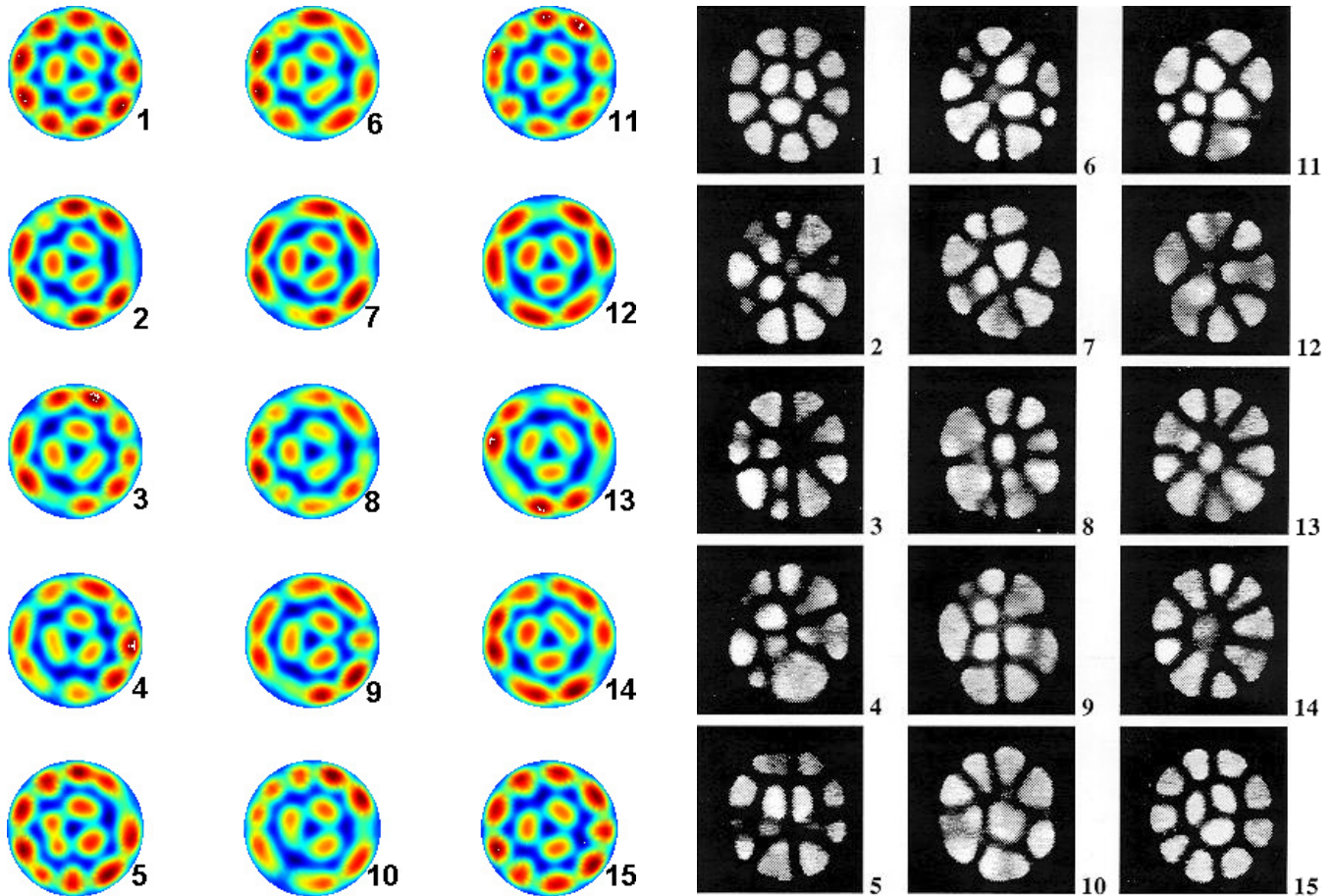


Fig. 13. (Left) For $R = 13.101$, $D = 0.00125$ and $\eta_{1,2,3}$, as in Fig. 4, noise-induced intermittent behavior in a two-ring state is observed in computer simulations of the Kuramoto–Sivashinsky model 1. Here, the transitions visit 9/3, 9/4, 10/4 and 6/3 two-ring states at intermittent intervals. (Right) A similar multiple-ring intermittent state found in laboratory experiments. Courtesy of M. Gorman at the University of Houston.

defined by $R = 13.101$, $D = 0.00125$ and $\eta_{1,2,3}$, as in Fig. 4. In principle, our analysis of the 1:2 mode interaction can be readily extended to study this more complex case of intermittency, except that the normal forms for this and many other cases have not yet been derived. The derivation of such normal forms is, however, in our plans for future work.

Acknowledgments

We would like to thank Michael Gorman for providing us with experimental data. This work was supported in part by National Science Foundation grants DMS-0504150 and CHE-0216563.

References

- Aboav, D. A. [1970] “The arrangement of grains in a polycrystal,” *Metallography* **3**, 383–390.
- Armbruster, D., Guckenheimer, J. & Holmes, P. [1988] “Heteroclinic cycles and modulated traveling waves in systems with $O(2)$ symmetry,” *Physica D* **29**, 257–282.
- Barrett, R., Berry, M., Chan, T. F. & Demmel, J. [1994] *Templates for the Solution of Linear Systems: Building Blocks for Iterative Methods*, eds. Donato, J., Dongarra, J., Eijkhout, V., Pozo, R., Romine, C. & Van der Vorst, H. (Society for Industrial and Applied Mathematics, Philadelphia, PA, 19104).
- Blomgren, P., Gasner, S. & Palacios, A. [2005a] “A stable second-order scheme for integrating the Kuramoto–Sivashinsky equation in polar coordinates,” *Phys. Rev. E* **72**, 036701.
- Blomgren, P., Gasner, S. & Palacios, A. [2005b] “Hopping behavior in the Kuramoto–Sivashinsky equation,” *Chaos* **15**, 013706.
- Carbone, A., Gromov, M. & Prusinkiewicz, P. (eds.) [1998] *Pattern Formation in Biology, Vision and Dynamics* (World Scientific, Singapore).
- Chaté, H. & Nicolaenko, B. [1990] “Phase turbulence, spatiotemporal intermittency and coherent

- structures,” *New Trends in Nonlinear Dynamics and Pattern Forming Phenomena* (Plenum, NY).
- Crank, J. & Nicolson, P. [1947] “A practical method for numerical evaluation of solutions of partial differential equations of the heat-conduction type,” *Proc. Cambridge Philos. Soc.* **43**, 60–64.
- Cross, M. C. & Hohenberg, P. C. [1993] “Pattern formation outside of equilibrium,” *Rev. Mod. Phys.* **65**, 851–1112.
- Dellnitz, M., Golubitsky, M. & Nicol, M. [1994] “Symmetry of attractors and the Karhunen–Loève decomposition,” *Trends and Perspectives in Applied Mathematics*, Vol. 100, ed. Sirovich, L., pp. 73–108.
- Dormer, K. J. [1980] *Fundamental Tissue Geometry for Biologists* (Cambridge University Press).
- Faraday, M. [1831] “On a peculiar class of acoustical figures; and on certain forms assumed by groups of particles upon vibrating elastic surfaces,” *Philos. Trans. R. Soc. London.* **121**, 299–340.
- Glazier, J. A. & Weaire, D. [1992] “The kinetics of cellular patterns,” *J. Phys.: Condens. Matter* **4**, 1867–1894.
- Gorman, M., el Hamdi, M. & Robbins, K. [1994] “Experimental observations of ordered states of cellular flames,” *Combust. Sci. and Tech.* **98**, 37–45.
- Graham, M. D., Lane, S. L. & Luss, D. [1993] “Proper orthogonal decomposition analysis of spatiotemporal temperature patterns,” *J. Phys. Chemistry* **97**, 889–894.
- Holmes, P., Lumley, J. L. & Berkooz, G. [1996] *Turbulence, Coherent Structures, Dynamical Systems and Symmetry* (Cambridge University Press).
- Hyman, J. M., Nicolaenko, B. & Zaleski, S. [1986] “Order and complexity in the Kuramoto–Sivashinsky model of weakly turbulent interfaces,” *Physica D* **23**, 265–292.
- Juel, A., Darbyshire, A. G. & Mullin, T. [1997] “The effect of noise on pitchfork and Hopf bifurcations,” *Proc. Math., Phys. and Eng. Sci.* **453**, 2627–2647.
- Karhunen, K. [1946] “Zur spektraltheorie stochastischer prozesse,” *Ann. Acad. Sci. Fennicae Ser. A* **37**, 3–76.
- Kepler, J. [1966] *A New Year’s Gift or on the Six-Cornered Snowflake* (Oxford University Press).
- Loève, M. [1955] *Probability Theory* (Van Nostrand, NY).
- Lumley, J. [1967] “The structure of inhomogeneous turbulent flows,” *Atmospheric Turbulence and Radio Wave Propagation*, eds. Yaglom, A. & Tatarski, V. (Nauka, Moscow), pp. 166–178.
- McNamara, B. & Wiesenfeld, K. [1988] “Theory of stochastic resonance,” *Phys. Rev. A* **39**, 4854–4869.
- Palacios, A., Gunaratne, G., Gorman, M. & Robbins, K. [1997] “Cellular pattern formation in circular domains,” *Chaos* **7**, 463–475.
- Palacios, A., Gunaratne, G., Gorman, M. & Robbins, K. [1998] “A Karhunen–Loève analysis of spatiotemporal flame patterns,” *Phys. Rev. E* **57**, 5958–5971.
- Pratt, K. W. [1991] *Digital Image Processing* (John Wiley, NY).
- Preisendorfer, R. [1988] *Principal Component Analysis in Meteorology and Oceanography* (Elsevier, Amsterdam).
- Reisz, F. & Sz.-Nagy, B. [1990] *Functional Analysis* (Dover Publications, NY).
- Sirovich, L. [1987a] “Turbulence and the dynamics of coherent structures, part i: Coherent structures,” *Q. Appl. Maths* **XLV**, 561–572.
- Sirovich, L. [1987b] “Turbulence and the dynamics of coherent structures, part ii: Symmetries and transformations,” *Q. Appl. Maths* **XLV**, 573–582.
- Sirovich, L. [1987c] “Turbulence and the dynamics of coherent structures, part iii: Dynamics and scaling,” *Q. Appl. Maths* **XLV**, 583–590.
- Stone, E. & Holmes, P. [1991] “Unstable fixed points, heteroclinic cycles and exponential tails in turbulence production,” *Phys. Lett. A* **155**, 29–42.
- Stone, E., Gorman, M., El-Hamdi, M. & Robbins, K. [1996] “Identification of intermittent ordered patterns as heteroclinic connections,” *Phys. Rev. Lett.* **76**, 2061–2064.
- Tsimring, L. S. & Aranson, I. S. [1997] “Localized and cellular patterns in a vibrated granular layer,” *Phys. Rev. Lett.* **79**, 0031-9007.
- van der Vorst, H. A. [1992] “A fast and smoothly converging variant of Bi-CG for the solution of nonsymmetric linear systems,” *SIAM J. Sci. Comput.* **13**, 631–644.
- Zhang, D., Wei, G., Kouri, D., Hoffmann, D., Palacios, A., Gorman, M. & Gunaratne, G. [1999] “Integrating the Kuramoto–Sivashinsky equation in a circular domain,” *Phys. Rev. E* **60**, 3353.

Appendix A

Modal Decomposition

In this appendix we provide a self-contained review of basic definitions and properties of the Proper Orthogonal Decomposition (POD) technique relevant to this work and discuss how the method can be applied to computer simulations in order to separate spatial and temporal behavior. The POD is a well-known technique for determining an optimal basis for the reconstruction of a data set [Karhunen, 1946; Loève, 1955]. It has been used in various disciplines that include fluid mechanics [Holmes *et al.*, 1996; Lumley, 1967], identification and control in chemical engineering [Graham *et al.*, 1993], oceanography [Preisendorfer, 1988], and image processing [Pratt, 1991]. Depending on the discipline, the POD is also known as

Karhunen-Loève decomposition, principal components analysis, singular systems analysis, or singular value decomposition.

A.1. Theoretical aspects

Let us consider a sequence of numerical and/or experimental observations represented by scalar functions $u(\mathbf{x}, t_i), i = 1, \dots, M$. Without loss of generality, the time-average of the sequence, defined by

$$\bar{u}(\mathbf{x}) = \langle u(\mathbf{x}, t_i) \rangle = \frac{1}{M} \sum_{i=1}^M u(\mathbf{x}, t_i), \quad (\text{A.1})$$

is assumed to be zero. The Proper Orthogonal Decomposition extracts time-independent orthonormal basis functions, $\Phi_k(\mathbf{x})$, and time-dependent orthonormal amplitude coefficients, $a_k(t_i)$, such that the reconstruction

$$u(\mathbf{x}, t_i) = \sum_{k=1}^M a_k(t_i) \Phi_k(\mathbf{x}), \quad i = 1, \dots, M \quad (\text{A.2})$$

is optimal in the sense that the average least squares truncation error

$$\varepsilon_m = \left\langle \left\| u(\mathbf{x}, t_i) - \sum_{k=1}^m a_k(t_i) \Phi_k(\mathbf{x}) \right\|^2 \right\rangle \quad (\text{A.3})$$

is minimized for any given number $m \leq M$ of basis functions over all possible sets of orthogonal functions. Here $\|\cdot\|$ is the L^2 -norm, $\|f\|^2 = (f, f)$, where (\cdot, \cdot) denotes the standard Euclidean inner product; $\langle \cdot \rangle$ denotes an average operation, usually over time; and the functions $\Phi_k(\mathbf{x})$ are called *empirical eigenfunctions*, *coherent structures*, or *POD modes*. In practice the state of a numerical model is only available at discrete spatial grid points, so that the observations that form the data set are vectors rather than continuous functions. In other words, $D = (x_1, x_2, \dots, x_N)$, where x_j is the j th grid point and $u(\mathbf{x}, t_i)$ is the vector $\mathbf{u}_i = [u(x_1, t_i), u(x_2, t_i), \dots, u(x_N, t_i)]^T$. The data set can be obtained from numerical simulation, experimental investigation or a combination of the numerical and experimental results. More importantly, it can be shown that the eigenfunctions Φ_k are the eigenvectors of the the tensor product matrix

$$S(\mathbf{x}, \mathbf{y}) = \frac{1}{M} \sum_{i=1}^M \mathbf{u}_i \mathbf{u}_i^T. \quad (\text{A.4})$$

A.2. Computational implementation: Method of snapshots

A popular technique for finding the eigenvectors of (A.4) is the *method of snapshots* developed by Sirovich [1987a, 1987b, 1987c]. It was introduced as an efficient method when the resolution of the spatial domain (N) is higher than the number of observations (M). The method of snapshots is based on the fact that the data vectors, \mathbf{u}_i , and the eigenvectors Φ_k , span the same linear space [Holmes et al., 1996; Sirovich, 1987a, 1987b, 1987c]. This implies that the eigenvectors can be written as a linear combination of the data vectors

$$\Phi_k = \sum_{i=1}^M v_i^k \mathbf{u}_i, \quad k = 1, \dots, M. \quad (\text{A.5})$$

After substitution in the eigenvalue problem, $S(\mathbf{x}, \mathbf{y})\Phi(\mathbf{y}) = \lambda\Phi(\mathbf{x})$, the coefficients v_i^k are obtained from the solution of

$$C\mathbf{v} = \lambda\mathbf{v}, \quad (\text{A.6})$$

where $\mathbf{v}^k = (v_1^k, \dots, v_M^k)$ is the k th eigenvector of (A.6), and C is a symmetric $M \times M$ matrix defined by $[c_{ij}] = (1/M)(\mathbf{u}_i, \mathbf{u}_j)$. Here (\cdot, \cdot) denotes the standard vector inner product, $(\mathbf{u}_i, \mathbf{u}_j) = u(x_1, t_i)u(x_1, t_j) + \dots + u(x_N, t_i)u(x_N, t_j)$. In this way the eigenvectors of the $N \times N$ matrix S (A.4) can be found by computing the eigenvectors of an $M \times M$ matrix C (A.6), a preferable task if $N \gg M$. The results presented in Sec. 3 were obtained with an implementation of the method of snapshots.

A.3. Properties of the POD decomposition

Since the kernel is Hermitian, $S(\mathbf{x}, \mathbf{y}) = S^*(\mathbf{y}, \mathbf{x})$, according to Riesz Theorem [Riesz, 1990], it admits a diagonal decomposition of the form

$$S(\mathbf{x}, \mathbf{y}) = \sum_{k=1}^N \lambda_k \Phi_k(\mathbf{x}) \Phi_k^*(\mathbf{y}). \quad (\text{A.7})$$

This fact is particularly useful when finding the POD modes analytically. They can be read off from the diagonal decomposition (A.7). Then the temporal coefficients, $a_k(t_i)$, are calculated by projecting the data set on each of the eigenfunctions

$$a_k(t_i) = (u(\mathbf{x}, t_i), \Phi_k(\mathbf{x})), \quad i = 1, \dots, M. \quad (\text{A.8})$$

It can be shown that both temporal coefficients and eigenfunctions are uncorrelated in time and space, respectively [Holmes et al., 1996; Sirovich,

1987a, 1987b, 1987c]. In addition, the POD modes $\{\Phi_k(\mathbf{x})\}$ and the corresponding temporal coefficients, $\{a_k(t_i)\}$, satisfy the following orthogonality properties

- (i) $\Phi_j^*(\mathbf{x})\Phi_k(\mathbf{x}) = \delta_{jk}$
- (ii) $\langle a_j(t_i)a_k^*(t_i) \rangle = \delta_{jk}\lambda_j$

where δ_{jk} represents the Kronecker delta function.

Property (ii) is obtained when the terms in the diagonal decomposition (A.7) are compared with the expression $S(\mathbf{x}, \mathbf{y}) = \sum \langle a_j(t_i)a_k^*(t_i) \rangle \times \Phi_j(\mathbf{x})\Phi_k^*(\mathbf{y})$. The non-negative and self-adjoint properties of $S(\mathbf{x}, \mathbf{y})$ imply that all eigenvalues are non-negative and can be ordered accordingly: $\lambda_1 \geq \lambda_2 \geq \dots \geq 0$. Statistically speaking, λ_k represents the variance of the data set in the direction of the corresponding POD mode, $\Phi_k(\mathbf{x})$. In physical terms, if u represents a component of a velocity field, then λ_k measures the amount of kinetic energy captured by the respective POD mode, $\Phi_k(\mathbf{x})$. In this sense, the energy measures the contribution of each mode to the overall dynamics.

The total energy captured in a proper orthogonal decomposition of a numerical or experimental data set is defined as the sum of all eigenvalues

$$E = \sum_{k=1}^M \lambda_k. \quad (\text{A.9})$$

The relative energy captured by the k th mode, E_k , is defined by

$$E_k = \frac{\lambda_k}{\sum_{j=1}^M \lambda_j}. \quad (\text{A.10})$$

Note that the cumulative sum of relative energies, $\sum E_k$, approaches one as the number of modes in the reconstruction increases to M . The relative phase-angle between two POD-time coefficients is defined by

$$\theta_{ij} = \arctan\left(\frac{a_i}{a_j}\right). \quad (\text{A.11})$$